
Modeling Uncertainty by Learning a Hierarchy of Deep Neural Connections

Raanan Y. Rohekar, Yaniv Gurwicz, Shami Nisimov, Gal Novik
Intel AI Lab

Abstract

Quantifying and measuring uncertainty in deep neural networks, despite recent important advances, is still an open problem. Bayesian neural networks are a powerful solution, where the prior over network weights is a design choice, often a normal distribution or other distribution encouraging sparsity. However, this prior is agnostic to the generative process of the input data, which might lead to unwarranted generalization for out-of-distribution tested data. We suggest treating the generative process of the input data as a confounder for the relation between the input and the discriminative function, thereby conditioning the prior of the network weights on the distribution of the input. We propose an algorithm for modeling this confounder through neural connectivity patterns. This approach is ultimately translated into a new deep architecture—a compact hierarchy of networks. We demonstrate that sampling networks from this hierarchy, proportionally to their posterior, is efficient and enables estimating various types of uncertainties. Empirical evaluations of our method demonstrate significant improvement compared to state-of-the-art calibration and out-of-distribution detection methods.

1 Introduction

Deep neural networks have become an important tool in applied machine learning, achieving state-of-the-art regression and classification accuracy in many domains. However, quantifying and measuring uncertainty in these discriminative models, despite recent important advances, is still an open problem. Representation of uncertainty is crucial for many domains, such as safety-critical applications, personalized medicine, and recommendation systems [7]. Common deep neural networks are not designed to capture model uncertainty, hence estimating it implicitly from the prediction is often inaccurate. Several types of uncertainties are commonly discussed [6, 19], where the two main types are: 1) epistemic uncertainty and 2) aleatoric uncertainty. Epistemic uncertainty is caused by the lack of knowledge, typically in cases where only a small training data exists, or for out-of-distribution inputs. Aleatoric uncertainty is caused by noisy data, and contrary to epistemic uncertainty, does not vanish in the large sample limit. In this work, we focus on two aspects of uncertainty, often required addressing in practical uses of neural networks: *calibration* [2] and *out-of-distribution* (OOD) detection.

Calibration is a notion that describes the relation between a predicted probability of an event and the actual proportion of occurrences of that event. It is generally measured using (strictly) *proper scoring rules* [8], such as negative log-likelihood (NLL) and the Brier score, both are minimized for calibrated models. Guo et al. [9] examined the calibration of recent deep architectures by computing the expected calibration error (ECE)—the difference between an approximation of the empirical reliability curve and the optimal reliability curve [21]. Miscalibration is often addressed by post processing the outputs [24, 9], approximating the posterior over the weights of a pre-trained network [25], or by learning an ensemble of networks [14, 18, 6, 17].

OOD detection is often addressed by designing a loss function to optimize during parameter learning of a given network architecture [19, 3]. Many of these methods are specifically tailored for detecting OOD, requiring some information about OOD samples, which is often impractical to obtain in real-world cases. In addition, these methods often are not capable of modeling different types of uncertainties. Ensemble methods, on the other hand, learn multiple sets of network parameters for a given structure [17], or approximate the posterior distribution over the weights from which they sample at test time [1, 18, 6].

In this paper, we make the distinction between *structure-based* methods, which include ensemble methods that replicate the structure or sample subsets from it, and *parameter-based* methods, which specify a loss function to be used for a given structure. Ensemble methods, in general, do not specify the loss function to be used for parameter learning, nor do they restrict post-processing of their output. It is interesting to note that while the majority of ensemble methods use distinct sets of parameters for each network [17], in the MC-dropout method [6] the parameters are shared across multiple networks. Common to all these methods is that they use a single network architecture (structure), as it is generally unclear how to fuse outputs from different structures. For example, it is required to know the prior distribution over structures.

We propose a method that samples network structures. Parts of one sampled structure may be similar to parts of another sampled structure but having different weights values, or different from each other. In addition, these structures may share some parts with other structures and their values (weight sharing), especially in the deeper layers. All these properties are learned from the input data.

2 Background

We focus on two approaches that are commonly used for modeling uncertainty: 1) Bayesian neural networks [6, 1], and 2) ensembles [17, 18]. Both approaches employ multiple networks to model uncertainty, where the main difference is the use/lack-of-use of shared parameters across networks during training and inference.

In Bayesian neural networks the weights, ϕ , are treated as random variables, and the posterior distribution is learned from the training data $p(\phi|\mathbf{x}, \mathbf{y})$. Then, the probability of label y^* for a test sample x^* is evaluated by

$$p(y^*|\mathbf{x}^*, \mathbf{x}, \mathbf{y}) = \int p(y^*|\mathbf{x}^*, \phi) p(\phi|\mathbf{x}, \mathbf{y}) d\phi. \quad (1)$$

However, since learning the posterior over ϕ and estimating Equation 1 are usually intractable, variational methods are often used, where an approximating variational distribution is defined $q(\phi)$, and the KL-divergence between the true posterior and the variational distribution, $\text{KL}(q(\phi) || p(\phi|\mathbf{X}, Y))$, is minimized.

A common practice is to set a prior $p(\phi)$,

$$p(\phi|\mathbf{X}, Y) = \frac{p(Y|\mathbf{X}, \phi) p(\phi)}{p(Y|\mathbf{X})}. \quad (2)$$

Thus, minimizing the KL-divergence is equivalent to maximizing a variational lower bound, Gal & Ghahramani [6] showed that the dropout objective, when applied before every layer, maximizes Equation ???. However, the prior $p(\phi)$ is a design choice and agnostic to the unlabeled data distribution $p(\mathbf{x})$, which may lead to unwarranted generalization for out-of-distribution test samples. As a remedy, in this work we propose to condition the parameters of the discriminative model, ϕ , on the unlabeled training data, \mathbf{X} . That is, to replace the prior $p(\phi)$ in Equation 2 with $p(\phi|\mathbf{x})$, thereby letting the unlabeled training data guide the posterior distribution rather than relying on some prior assumption over the prior.

3 A Hierarchy of Deep Neural Networks

We first describe the key idea, then introduce a new neural architecture, and finally, describe a stochastic inference algorithm for estimating different types of uncertainties.

3.1 Key Idea

We approximate the prediction, Equation 1, by sampling from the posterior, $\tilde{\phi}_i \sim p(\phi|\mathbf{x}, \mathbf{y})$,

$$P(y^*|\mathbf{x}^*, \mathbf{x}, \mathbf{y}) \approx \frac{1}{m} \sum_{i=1}^m P(y^*|\mathbf{x}^*, \tilde{\phi}_i). \quad (3)$$

Since sampling from the posterior is intractable for deep neural networks, we follow a Bayesian approach and propose a prior distribution for the parameters. However, in contrast to the common practice of assuming a Gaussian distribution (or some other prior independent of the data), our prior depends on the unlabeled training data, $p(\phi|\mathbf{x})$.

We define $p(\phi|\mathbf{x})$ by first, considering a generative model for \mathbf{x} , with parameters θ . Next, we assume a dependency relation between θ and ϕ , such that the joint distribution factorizes as

$$p(X, Y, \phi, \theta) = p(Y|X, \phi) p(X|\theta) p(\phi|\theta) p(\theta). \quad (4)$$

In essence, we assume a generative process of \mathbf{X} , to confound the relation $\mathbf{X} \rightarrow \phi$ conditioned on Y . That is, in contrast to the common practice where a “v-structure” is assumed, $\mathbf{X} \rightarrow Y \leftarrow \phi$, we assume a generative function, parametrized by θ , to be a parent of \mathbf{X} and ϕ , as illustrated in Figure 1.

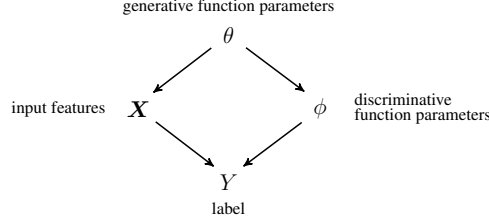


Figure 1: Our assumptions described as a causal diagram.

Thus, using the prior $p(\phi|\theta)$ is expected to diminish unwarranted generalization for out-of-distribution samples, i.e., samples with low $p_\theta(\mathbf{X})$. As these samples are non-present or scarce in the training set, they have non or diminished influence on ϕ . It follows that the posterior is

$$p(\phi|\mathbf{x}, \mathbf{y}) \propto \int p(\mathbf{y}|\mathbf{x}, \phi) p(\phi|\theta) p(\theta|\mathbf{x}) d\theta. \quad (5)$$

Two main questions arise: 1) what generative model should be used, and 2) how can we define the conditional relation $p(\phi|\theta)$. It is desired to define a generative model such that the conditional distribution $p(\phi|\theta)$ can be computed efficiently.

Our solution includes a new deep model, which we call BRAINet, where its structure (inter-layer neural connectivity pattern), is learned and scored from unlabeled training data, \mathbf{x} . From BRAINet, multiple generative structures, $\{\tilde{\mathcal{G}}_1, \tilde{\mathcal{G}}_2, \tilde{\mathcal{G}}_3, \dots\}$, can be sampled from their posterior $p(\tilde{\mathcal{G}}|\mathbf{x})$ during training and inference, where in our case $p(\theta_i|\mathbf{x}) \equiv p(\tilde{\mathcal{G}}_i|\mathbf{x})$. This can be described as using multiple networks during inference and training (similar to MC-dropout [6] and Deep Ensembles [17]). However, as these structures are sampled from a single network, they may share some of their parameters, especially in deeper layer. This is different from MC-dropout where all the parameters are shared across networks, and Deep Ensembles where none of the parameters are shared.

3.2 BRAINet: A Hierarchy of Deep Networks

Recently, Rohekar et al. [27] introduced an algorithm, called B2N, for learning the structure, \mathcal{G} , of discriminative deep neural networks in an unsupervised manner. The B2N algorithm, learns an inter-layer connectivity pattern, where neurons in a layer may connect to other neurons in any deeper layer, not just to the ones in the next layer.

Initially, B2N learns a deep generative graph $\tilde{\mathcal{G}}$ with latent nodes \mathbf{H} . This graph is constructed by unfolding the recursive calls in the RAI structure learning algorithm [30]. RAI learns a Bayesian

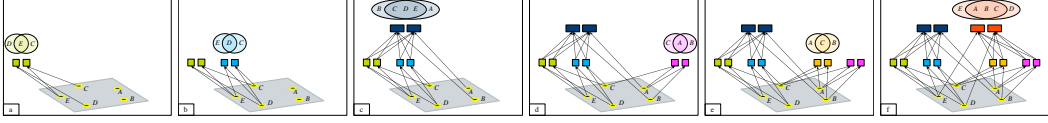


Figure 2: An example for learning the structure of a BRAINet with $s = 2$. Network inputs, $\{A, \dots, E\}$, are depicted on the gray plain. Each rectangle (or square) represents a layer of neurons (denoted L_i^t in Algorithm 1-line 14). The Venn diagram, above each set of rectangles, represents the field-of-view each rectangle (layer) has over the input. The group $\{C, D, E\}$ is decomposed in two ($s = 2$) ways: (a) $X_{A1} = D, X_{A2} = C, X_D = E$, and (b) $X_{A1} = E, X_{A2} = C, X_D = D$. Each decomposition results in a different connectivity pattern, green rectangles in (a) and light-blue rectangles in (b). Next, (c) represents returning to the calling function, where $X_{A1} = B, X_{A2} = A, X_D = \{C, D, E\}$. Similarly, a different decomposition of the input X is demonstrated in (d), (e), and (f). Finally, a label node Y is added as a child of the deepest layers.

network¹ structure \mathcal{B} , encoding $p(\mathbf{X})$, and the B2N learns a deep generative graph such that,

$$p_{\mathcal{B}}(\mathbf{X}) = \int p_{\tilde{\mathcal{G}}}(\mathbf{X}, \mathbf{H}) d\mathbf{H}. \quad (6)$$

Interestingly, a discriminative network structure \mathcal{G} is proved to mimic a deep generative structure $\tilde{\mathcal{G}}$, having the exact same structure for (\mathbf{X}, \mathbf{H}) . That is, for any θ' , there exists ϕ' , which can produce the posterior distribution over the latent variables in the generative model, $p_{\theta'}(\mathbf{H}|\mathbf{X}) = p_{\phi'}(\mathbf{H}|\mathbf{X}, Y)$ ².

Recently, an extension for the RAI algorithm [30] was proposed, called B-RAI [26]. B-RAI is a Bayesian approach that learns multiple Bayesian network structures (not to be confused with Bayesian neural networks), scores them and couples them into a hierarchy. This hierarchy is represented by a tree, which they call GGT. The Bayesian scores of each structure is encoded efficiently in the GGT, which allows structures, \mathcal{B} , to be sampled from this GGT according to their posterior distribution, $P(\mathcal{B}|\mathbf{X})$. Based on the principles behind the B2N algorithm, we propose converting this Bayesian network GGT (generated by B-RAI) into a deep neural network hierarchy. We call this hierarchy B-RAI neural network, abbreviated to BRAINet. Then, a neural network structure, \mathcal{G} , can be sampled from the BRAINet model proportionally to $P(\mathcal{B}|\mathbf{X})$, where \mathcal{G} has the same connectivity as a generative structure $\tilde{\mathcal{G}}$, and where the relation in Equation 6 holds. This yields a dependency between an implicit generative model for the data, $P(\mathbf{X})$ and the discriminative structure, $P(Y|\mathbf{X})$.

3.2.1 BRAINet Structure Learning

Before describing the structure learning algorithm, we define important concepts, in the field on Bayesian network structure learning, introduced by Yehezkel & Lerner [30].

Definition 1 (Autonomous set of nodes). *In a graph defined over \mathbf{X} , a set of nodes $\mathbf{X}' \subseteq \mathbf{X}$ is called autonomous given $\mathbf{X}_{\text{ex}} \subset \mathbf{X}$ if the parents' set, $\text{Pa}(\mathbf{X})$, $\forall \mathbf{X} \in \mathbf{X}'$ is $\text{Pa}(\mathbf{X}) \subset \mathbf{X}' \cup \mathbf{X}_{\text{ex}}$.*

Definition 2 (d-separation resolution). *The resolution of a d-separation relation between a pair of non-adjacent nodes in a graph is the size of the smallest condition set that d-separates the two nodes.*

Definition 3 (d-separation resolution of a graph). *The d-separation resolution of a graph is the highest d-separation resolution in the graph.*

We present a recursive algorithm, Algorithm 1, for learning the structure of a BRAINet model. Each recursive call receives a Bayesian network structure \mathcal{B} , a set of endogenous \mathbf{X} and exogenous \mathbf{X}_{ex} nodes, and a target conditional independence order n . The Bayesian network structure encodes $P(\mathbf{X}|\mathbf{X}_{\text{ex}})$, providing an efficient factorization of this distribution. The d-separation resolution of \mathcal{B} is assumed $n - 1$.

At the beginning of each recursive call, an exit condition is tested (line 2). This condition is satisfied if conditional independence of order n cannot be tested (a conditional independence order is defined to be the size of the condition set). In this case, the maximal depth is reached and an empty graph is

¹Not to be confused with Bayesian neural network.

²As the structures of $\tilde{\mathcal{G}}$ and \mathcal{G} are identical, differing only in edge direction, we assume a one-to-one mapping from each latent node in $\tilde{\mathcal{G}}$ to its corresponding latent node in \mathcal{G} .

Algorithm 1: BRAINet structure learning

```

1 BRAINet_SL ( $\mathcal{B}, \mathbf{X}, \mathbf{X}_{\text{ex}}, n$ )
   Input: an initial CPDAG  $\mathcal{B}$  over endogenous  $\mathbf{X}$  & exogenous  $\mathbf{X}_{\text{ex}}$  observed variables, and a desired
       resolution  $n$ .
   Output:  $L$ , the deepest layer in a learned structure

2   if the maximal indegree of  $\mathbf{X}$  in  $\mathcal{B}$  is lower than  $n + 1$  then                                ▷ exit condition
3      $p := \text{Score}(\mathbf{X}|\mathcal{B})$                                                                 ▷ a Bayesian score (e.g., BDeu)
4      $L :=$  a gather layer for  $\mathbf{X}$  with score  $p$ 
5     return  $L$ 

6   for  $t = 1 : s$  do
7      $\mathbf{x}^* :=$  sample with replacement from training data  $\mathbf{x}$                                 ▷ bootstrap sample
8      $\mathcal{B}^* := \text{IncSeparation}(\mathcal{B}, n, \mathbf{x}^*)$                                                 ▷ increase d-separation resolution to  $n$ 
9      $\{\mathbf{X}_D, \mathbf{X}_{A_1}, \dots, \mathbf{X}_{A_k}\} := \text{FindAutonomous}(\mathbf{X}|\mathcal{B}^*)$                         ▷ decompose
10    for  $i = 1 : k$  do
11       $L_{A_i} := \text{BRAI\_NN\_SL}(\mathcal{B}^*, \mathbf{X}_{A_i}, \mathbf{X}_{\text{ex}}, n + 1)$                             ▷ recursively call for ancestors
12     $L_D := \text{BRAI\_NN\_SL}(\mathcal{B}^*, \mathbf{X}_D, \mathbf{X}_{\text{ex}} \cup \{\mathbf{X}_{A_i}\}_{i=1}^k, n + 1)$                 ▷ recursively call for descendant
13    Create an empty layer container  $L^t$  (tagged with index  $t$ )
14    In  $L^t$  create  $k$  independent layers:  $L_1^t, \dots, L_k^t$ 
15     $\forall i \in \{1, \dots, k\}$ , connect:  $L_{A_i} \rightarrow L_i^t \leftarrow L_D$                                 ▷ connect
16  return  $L = \{L^t\}_{t=1}^s$ 

```

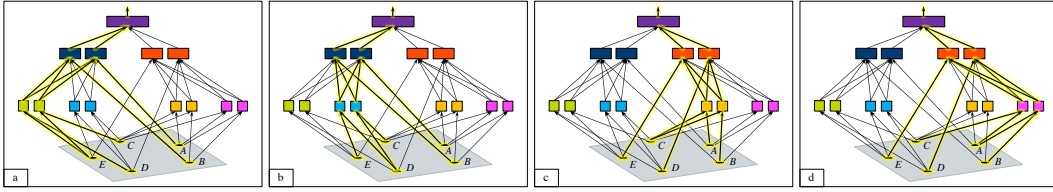


Figure 3: Stochastic training/inference in a BRAINet model. In a single stochastic/training step, a subset of the network is selected. In this example, there are four possible sub-network selections: a, b, c, and d. Network inputs, A, \dots, E , are depicted on a gray plain. A rectangle represents a layer of neuron, an edge represents dense connectivity—every element in the origin is connected to every element in the destination. Note that, in every stochastic step (a, b, c, d), all the inputs are selected, and each input is selected only once.

returned (a gather layer composed of observed nodes). From this point, the recursive procedure will trace back, adding latent parent layers. Each recursive call consists of three stages:

- a) Using a bootstrap sample of the training data, increase the d-separation resolution of \mathcal{B} to n . Then decompose the input features, \mathbf{X} , into autonomous sets of nodes (lines 7–9): one descendant set, \mathbf{X}_D , and k ancestor sets, $\{\mathbf{X}_{A_i}\}_{i=1}^k$, such that $p(\mathbf{X}|\theta) = p(\mathbf{X}_D|\mathbf{X}_{A_1}, \dots, \mathbf{X}_{A_k}) \prod_{i=1}^k p(\mathbf{X}_{A_i})$.
- b) Call recursively to learn BRAINet structures for each autonomous set (lines 10–12).
- c) Merge the returned BRAINet structures into a single structure (lines 13–15).

These stages are executed s times (line 6), resulting in an ensemble of s BRAINet structures. The deepest layers, $\{L^1, \dots, L^s\}$, of these structures are grouped together (line 16), while maintaining their index $1, \dots, s$ in L , and returned. Note that the caller function treats this group as a single layer. A detailed description of Algorithm 1 can be found in Appendix A, and complexity analysis in Appendix B. An example for learning a BRAINet structure with $s = 2$ (each recursive call returns an ensemble of two BRAINet models) is given in Figure 2.

3.2.2 BRAINet Training and Inference

The BRAINet model allows us to sample sub-networks with respect to their relative posterior probability. The scores calculation and sub-network selection are performed recursively, from the

leaves to the root. For each autonomous set, given s sampled sub-networks and their scores returned from s recursive calls, one of the s results is sampled. We use the Boltzmann distribution,

$$P(t; \{sc^{t'}\}_{t'=1}^s) = \frac{\exp[sc^t/\gamma]}{\sum_{t'=1}^s \exp[sc^{t'}/\gamma]}, \quad (7)$$

where γ is a “temperature” term. When $\gamma \rightarrow \infty$, results are sampled from a uniform distribution, and when $\gamma \rightarrow 0$ the index of the maximal value is selected ($\arg \max$). We use $\gamma = 1$ and the Bayesian score, BDeu [11]. Finally, the sampled sub-networks, each corresponding to an autonomous set, are merged. The score of the resulting network is the sum of scores³ of all autonomous sets merged into the network. When training the parameters, at each step, a single sub-network is sampled using a uniform distribution and its weights are updated. At inference, however, there are two options. In the first, which we call “stochastic”, we run T forward passes, each time sampling a single network with respect to Equation 7. Finally, the outputs of the sampled networks are averaged. Figure 3 illustrates several forward passes sampled from the BRAINet model. This is similar to dropout at inference, except that a sub-network is sampled with respect to its posterior. Note that, in BRAINet, in contrast to MC-dropout, weights are not sampled independently, and there is an implicit dependency between sampling probabilities. In the second inference option, which we call “simultaneous”, we run a single forward pass through the BRAINet and recursively perform a weighted average of the s activations for each autonomous set.

3.2.3 BRAINet Uncertainty Estimation

Several measures of uncertainty can be computed using the BRAINet model. Firstly, the max-softmax [28] and entropy [6] can be computed on the outputs of a single “simultaneous” forward pass or on the average of outputs from multiple stochastic forward passes. Secondly, using the distinct outputs of multiple forward passes, we can compute the expected entropy, $\mathbb{E}_{p(\phi|\mathbf{x},\mathbf{y})} \mathcal{H}[p(y^*|x^*, \phi)]$, or the mutual information, $\text{MI}(y^*, \phi|x^*, \mathbf{x}, \mathbf{y})$, [29]. In Appendix C-Figure 2, we qualitatively show epistemic uncertainty estimation using MI, calculated from the BRAINet model, for images generated by VAE [16] trained on MNIST. In addition, using the outputs of multiple stochastic passes, we can estimate the distribution over the network output. Finally, we demonstrate an interesting property of our method that learns a broader prior over ϕ as the training set size decreases. That is, a relation between the predictive uncertainty and the number of unique structures (connectivity patterns) encoded in a BRAINet model (exemplified in Appendix C-Figure 1).

4 Empirical Evaluation

BRAINet structure learning algorithm is implemented using BNT [20] and runs efficiently on a standard desktop CPU. In all the experiments, we used ReLU activations, ADAM [15] optimization, and batch normalization [13] for all the dense layers. Unless otherwise stated, each experiment was repeated 10 times. Mean and STDev on test-set are reported. Code is available in the Appendix.

4.1 An Ablation Study for Evaluating the Effect of Confounding with a Generative Process

First, we conduct an ablation study by gradually reducing the dependence of the discriminative parameters ϕ on the generative parameters θ , i.e., the strength of the link $\theta \rightarrow \phi$ in Figure 1, and measuring the performance of the resulting model. In the extreme case of disconnecting this link, the BRAINet structure will simply become a Deep Ensembles model [17] with s independent networks. Figure 4 demonstrates that even for a small dependence between θ and ϕ , as restricted by BRAINet, a significant improvement is achieved in performance. X -axis represents the strength of the link $\theta \rightarrow \phi$ (see Figure 1), where the values represent the amount of mutual information that is required for a pair of nodes in \mathbf{X} to be considered dependent (line 8, Algorithm 1). When this value is low, all the nodes in \mathbf{X} are considered dependent and no structure is learned. For a mutual information threshold of 0, a simple ensemble of s networks is obtained where each network is composed of stacked fully connected layer.

³Using a decomposable score, such as BDeu, the score of a Bayesian network is $sc = \sum_{i=1}^n sc(X_i|Pa_i)$.

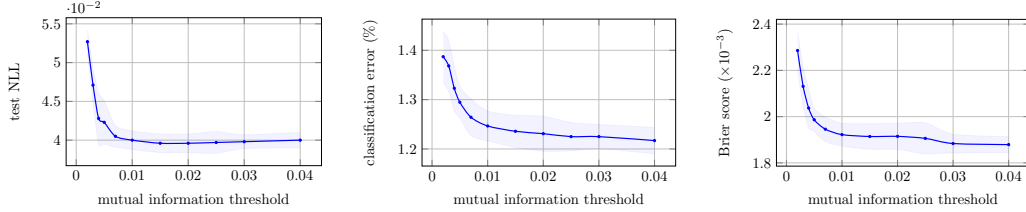


Figure 4: Results of an ablation study. The effect of conditioning the discriminative function on the generative process, $p(\phi|\theta)$ as measured by the test NLL, classification error, and Brier score. It is evident that performance worsens after weakening the dependence of ϕ on θ .

4.2 Calibration

BRAINet can be perceived as a compact representation of ensembles. We demonstrate on MNIST that it achieves higher classification accuracy and is better calibrated than Deep Ensembles for the same model size (Figure 5). Here, we used the simultaneous inference mode of BRAINet. Next, we evaluate the accuracy and calibration of BRAINet as a function of stochastic forward passes, and find it to significantly outperforms Bayes-by-Backprop [1] and MC-dropout (Figure 6). We also find that using the BRAINet structure within either Deep Ensembles or with MC-dropout methods, further improves these later approaches. For that we use common UCI-repository [4] regression benchmarks. Results are reported: Appendix D-Table 1 for Deep Ensembles, and Appendix D-Table 2 for MC-dropout. Finally, we compare BRAINet to various state-of-the-art methods on large networks. In all benchmarks, BRAINet achieves the lowest expected calibration error [9] (Appendix D-Table 3).

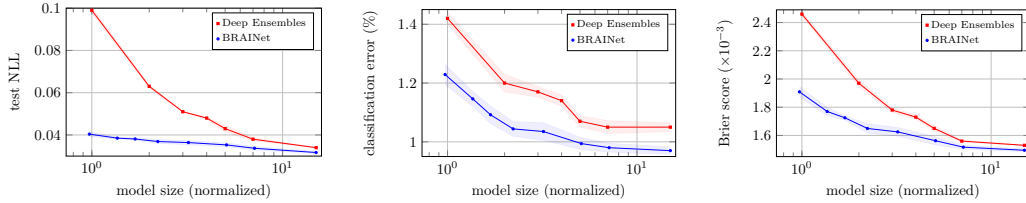


Figure 5: Performance as a function of normalized model size. Test NLL, classification error, and Brier score of BRAINet, compared to Deep Ensembles [17]. X-axis is the model size divided by the size of a single network (240K parameters) in the Deep Ensembles model. For BRAINet, up to model size 5, $s = 2$, and from model size 7 and above, $s = 3$. Different BRAINet sizes, for a given s , are obtained by varying the number of neurons in the dense-layers.

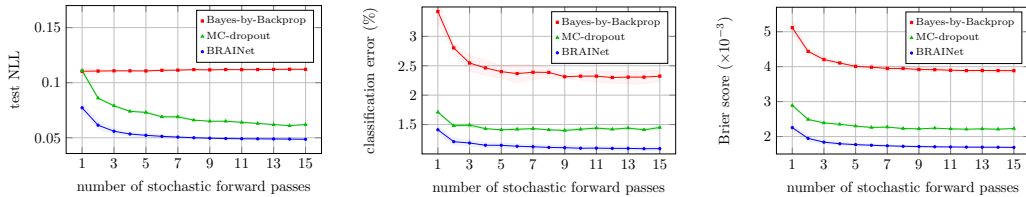


Figure 6: Performance as a function of the number of forward passes (number of sampled networks). Test NLL, classification error, and Brier score of BRAINet, compared to MC-dropout [6] and Bayes-by-Backprop [1]. We used a BRAINet with $s = 2$. Model size is 240K parameters for MC-dropout and BRAINet, and double for Bayes-by-Backprop.

4.3 Out-of-Distribution Detection

Next, we evaluate the the performance of detecting OOD samples using the BRAINet structure. First, we compare it to a baseline network and MC-dropout (We found MC-dropout to significantly outperform Bayes-by-Backprop and Deep Ensembles on this task). In order to evaluate the gain in

performance resulting only from the structure, we use the cross-entropy loss for parameter learning. Using other loss functions that are suited for improving OOD detection [19], may further improve the results (see the next experiment). In this experiment we used a ResNet-20 network [10], pre-trained on CIFAR-10 data. For MC-dropout, we used a structure having 2 fully-connected layers, and for BRAINet, we learned a 2-layer structure with $s = 2$. Both structures have 16K parameters and they replace the last layer of ResNet-20. SVHN dataset [22] is used as the OOD samples. We calculated the area under the ROC and precision-recall curves, treating OOD samples as positive classes (Table 1).

Table 1: OOD detection (SVHN dataset) by replacing the last layer of ResNet20, pre-trained on CIFAR-10, with a learned structure. Parameters are trained using cross-entropy loss. Two inference mode of BRAINet: a single simultaneous forward pass (BRAINet sm.), and multiple stochastic forward passes. MC-dropout and BRAINet use 15 forward passes (see also Appendix D-Figure 3).

METHOD	ERR	AUC-ROC				AUC-PR			
		MAX. P	ENT.	MI	E.ENT.	MAX. P	ENT.	MI	E.ENT.
BASILINE	7.7	90.38	90.74	—	—	93.94	94.09	—	—
BRAINET SM.	8.0	91.62	92.18	—	—	94.91	94.80	—	—
MC-DROPOUT	8.2	90.73	90.26	84.74	90.61	94.31	93.71	88.89	94.46
	± 0.1	± 0.78	± 0.81	± 1.07	± 0.93	± 0.33	± 0.34	± 0.45	± 0.46
BRAINET	7.5	92.13	92.61	91.87	92.98	95.37	95.36	94.6	95.64
	± 0.1	± 0.15	± 0.03	± 0.13	± 0.10	± 0.13	± 0.07	± 0.25	± 0.05

Lastly, we demonstrate that training the parameters of BRAINet using a loss function, specifically designed for OOD detection [3], achieves a significant improvement over a common baseline [12] and improves state-of-the art results (Table 2).

Table 2: OOD detection by training BRAINet parameters using a loss function designed for OOD detection. A comparison between a baseline [12], confidence-based thresholding [3], and BRAINet with the same confidence measure. Architecture: VGG-13, in-distribution: CIFAR-10, OOD: TinyImageNet. BRAINet replaces the last layer. FPR @TPR=95%: false positive rate at true positive rate of 95%. Detection error: minimum classification error over all possible thresholds. AUC-ROC and AU-PR: area under ROC and precision-recall curves. “in”/“out” indicate that in/out-of-distribution data is the positive class. An arrow indicates if lower (\downarrow) or higher (\uparrow) is better.

MEASURE		BASILINE [12]	CONFIDENCE [3]	BRAINET
CLASSIFICATION ERROR	\downarrow	5.28	5.63	5.65
FPR @TPR=95%	\downarrow	0.438	0.195	0.124
DETECTION ERROR	\downarrow	0.120	0.092	0.076
AUC-ROC	\uparrow	0.935	0.970	0.980
AUC-PR (IN)	\uparrow	0.946	0.974	0.982
AUC-PR (OUT)	\uparrow	0.917	0.965	0.979

5 Conclusions

We propose a method for confounding the training process in deep neural networks, conditioning on the distribution of the input. This leads to a new architecture—BRAINet: a hierarchy of neural networks. From this hierarchy, neural network structures can be sampled from their posterior. Using an ablation study, we found that even slightly conditioning on the generative process of the input improves performance. In addition, We found that the number of neural connectivity patterns in BRAINet is adjusted automatically according to the uncertainty in the input training data. We demonstrated that this enables estimating different types of uncertainties, better than common and state-of-the-art methods, as well as higher accuracy on both small and large datasets. We conjecture that the resulting model can also be effective at detecting adversarial attacks, where an adversarial attack can be interpreted as an intervention on the input data, thereby modifying our assumed causal structure. We plan to explore this in our future work.

References

- [1] Blundell, C., Cornebise, J., Kavukcuoglu, K., and Wierstra, D. Weight uncertainty in neural network. In *International Conference on Machine Learning (ICML)*, pp. 1613–1622, 2015.
- [2] Dawid, A. P. The well-calibrated Bayesian. *Journal of the American Statistical Association*, 77(379): 605–610, 1982.
- [3] DeVries, T. and Taylor, G. W. Learning confidence for out-of-distribution detection in neural networks. *arXiv preprint arXiv:1802.04865*, 2018.
- [4] Dua, D. and Graff, C. UCI machine learning repository, 2017. URL <http://archive.ics.uci.edu/ml>.
- [5] Efron, B. and Tibshirani, R. J. *An introduction to the bootstrap*. CRC press, 1994.
- [6] Gal, Y. and Ghahramani, Z. Dropout as a Bayesian approximation: Representing model uncertainty in deep learning. In *international conference on machine learning (ICML)*, pp. 1050–1059, 2016.
- [7] Ghahramani, Z. Probabilistic machine learning and artificial intelligence. *Nature*, 521(7553):452, 2015.
- [8] Gneiting, T. and Raftery, A. E. Strictly proper scoring rules, prediction, and estimation. *Journal of the American Statistical Association*, 102(477):359–378, 2007.
- [9] Guo, C., Pleiss, G., Sun, Y., and Weinberger, K. Q. On calibration of modern neural networks. In *International Conference on Machine Learning (ICML)*, pp. 1321–1330, 2017.
- [10] He, K., Zhang, X., Ren, S., and Sun, J. Deep residual learning for image recognition. In *Proceedings of the IEEE conference on computer vision and pattern recognition*, pp. 770–778, 2016.
- [11] Heckerman, D., Geiger, D., and Chickering, D. M. Learning Bayesian networks: The combination of knowledge and statistical data. *Machine learning*, 20(3):197–243, 1995.
- [12] Hendrycks, D. and Gimpel, K. A baseline for detecting misclassified and out-of-distribution examples in neural networks. *International Conference on Learning Representations (ICLR)*, 2017.
- [13] Ioffe, S. and Szegedy, C. Batch normalization: Accelerating deep network training by reducing internal covariate shift. In *International Conference on Machine Learning*, pp. 448–456, 2015.
- [14] Izmailov, P., Podoprikin, D., Garipov, T., Vetrov, D., and Wilson, A. G. Averaging weights leads to wider optima and better generalization. *arXiv preprint arXiv:1803.05407*, 2018.
- [15] Kingma, D. and Ba, J. Adam: A method for stochastic optimization. In *Proceedings of the International Conference on Learning Representations (ICLR)*, 2015.
- [16] Kingma, D. P. and Welling, M. Auto-encoding variational bayes. In *Proceedings of the International Conference on Learning Representations (ICLR)*, 2014.
- [17] Lakshminarayanan, B., Pritzel, A., and Blundell, C. Simple and scalable predictive uncertainty estimation using deep ensembles. In *Advances in Neural Information Processing Systems (NIPS)*, pp. 6402–6413, 2017.
- [18] Maddox, W., Garipov, T., Izmailov, P., Vetrov, D., and Wilson, A. G. A simple baseline for Bayesian uncertainty in deep learning. *arXiv preprint arXiv:1902.02476*, 2019.
- [19] Malinin, A. and Gales, M. Predictive uncertainty estimation via prior networks. In *Advances in Neural Information Processing Systems (NeurIPS)*, 2018.
- [20] Murphy, K. The Bayes net toolbox for Matlab. *Computing Science and Statistics*, 33:331–350, 2001.
- [21] Naeini, M. P., Cooper, G., and Hauskrecht, M. Obtaining well calibrated probabilities using bayesian binning. In *Twenty-Ninth AAAI Conference on Artificial Intelligence*, 2015.
- [22] Netzer, Y., Wang, T., Coates, A., Bissacco, A., Wu, B., and Ng, A. Y. Reading digits in natural images with unsupervised feature learning. In *NIPS workshop on deep learning and unsupervised feature learning*, 2011.
- [23] Pearl, J. *Causality: Models, Reasoning, and Inference*. Cambridge university press, second edition, 2009.
- [24] Platt, J. et al. Probabilistic outputs for support vector machines and comparisons to regularized likelihood methods. *Advances in large margin classifiers*, 10(3):61–74, 1999.

- [25] Ritter, H., Botev, A., and Barber, D. A scalable laplace approximation for neural networks. 2018.
- [26] Rohekar, R. Y., Gurwicz, Y., Nisimov, S., Koren, G., and Novik, G. Bayesian structure learning by recursive bootstrap. In *Advances in Neural Information Processing Systems (NeurIPS)*, 2018.
- [27] Rohekar, R. Y. Y., Nisimov, S., Gurwicz, Y., Koren, G., and Novik, G. Constructing deep neural networks by Bayesian network structure learning. In *Advances in Neural Information Processing Systems (NeurIPS)*, 2018.
- [28] Shiyu, L., Yixuan, L., and R., S. Enhancing the reliability of out-of-distribution image detection in neural networks. In *Proceedings of the International Conference on Learning Representations (ICLR)*, 2018.
- [29] Smith, L. and Gal, Y. Understanding Measures of Uncertainty for Adversarial Example Detection. In *Uncertainty in Artificial Intelligence (UAI)*, 2018.
- [30] Yehezkel, R. and Lerner, B. Bayesian network structure learning by recursive autonomy identification. *Journal of Machine Learning Research (JMLR)*, 10(Jul):1527–1570, 2009.

Appendix

A BRAINet Structure Learning: A Detailed Description

In this section we provide a detailed description of Algorithm 1 and its three main stages. For more details, specific to Bayesian networks (not to be confused with Bayesian neural networks), refer to Pearl [23].

Stage a. First in line 7, a bootstrap sample \mathbf{x}^* is created by sampling-with-replacement from the training data, \mathbf{x} (non-parametric bootstrap). The bootstrap principle is a common approach used to approximate a population distribution by a sample distribution [5].

Next in line 8, the bootstrap sample \mathbf{x}^* is used for learning a Bayesian network structure \mathcal{B}^* , with sparser connectivity than \mathcal{B} , such that \mathcal{B} can mimic \mathcal{B}^* , $\mathcal{B}^* \preceq \mathcal{B}$ [23]. That is, for every set of parameters ν , quantifying \mathcal{B} , there exists a set of parameters ν^* , quantifying \mathcal{B}^* , such that $p_{\mathcal{B},\nu}(X) = p_{\mathcal{B}^*,\nu^*}(X)$. The \mathcal{B}^* structure is learned by testing conditional independence of order n between pairs of nodes connected in \mathcal{B} . That is, $X \perp\!\!\!\perp X' | \mathcal{S}$ for every connected pair $X \in \mathbf{X}$ and $X' \in \mathbf{X}_{\text{ex}}$ given a condition set $\mathcal{S} \subset \{\mathbf{X}_{\text{ex}} \cup \mathbf{X}\}$ of size n . Edges between conditionally independent nodes are then removed, and the remaining edges are directed by applying two rules. First, v-structures are identified and directed. Then, edges are continually directed, by avoiding the creation of new v-structures and directed cycles, until no more edges can be directed. Following the definition of Yehezkel & Lerner [30] for d-separation resolution, we say that this function increases the graph d-separation resolution from $n - 1$ to n .

Finally in line 9, the procedure `SplitAutonomous` (line 7) identifies autonomous sets: one descendant set, \mathbf{X}_{D} , and k ancestor sets, $\mathbf{X}_{\text{A}1}, \dots, \mathbf{X}_{\text{A}k}$. This decomposition is achieved in two steps. First, the nodes having the lowest topological order (nodes without outgoing directed edges) are grouped into \mathbf{X}_{D} , and then, \mathbf{X}_{D} is removed (temporarily) from \mathcal{B} revealing unconnected sub-structures. The number of unconnected sub-structures is denoted by k and the nodes set of each sub-structure is denoted by $\mathbf{X}_{\text{A}i}$ ($i \in \{1 \dots k\}$).

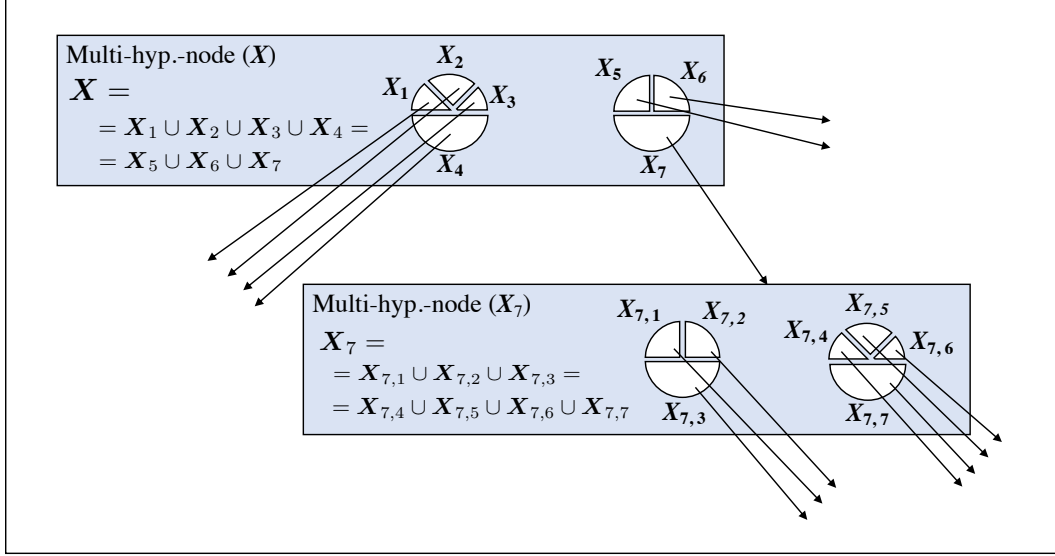
Stage b. The BRAINet structure learning algorithm is recursively called for each autonomous (line 11) and descendant (line 12) set. An autonomous set in \mathcal{B} includes all its nodes' parents (complying with the Markov property) and thus, the algorithm can be called recursively and independently. Each recursive call returns a BRAINet model: $L_{\text{A}i}$ for each ancestor set $\mathbf{X}_{\text{A}i}$, and L_{D} for the descendant set \mathbf{X}_{D} . Note that, each recursive call, has a smaller field-of-view (FOV) over the input \mathbf{X} compared to its caller function ($\mathbf{X}_{\text{A}i} \subset \mathbf{X}$).

Stage c. BRAINet models returned from the recursive calls are merged by connecting the deepest layer of each of them in the following manner. First in line 13, a layer container is created, denoted by L^t , where t is an index created in line 6 and represents one of s bootstrap-created splits. Next in line 14, for the i -th BRAINet model, created for ancestor set $\mathbf{X}_{\text{A}i}$, a layer of neurons, L_i^t is created. Finally in line 15, the BRAINet models returned from the recursive calls are connected. The deepest layer of L_{D} is connected to all the newly created layers L_1^t, \dots, L_k^t and the deepest layer of the i -th BRAINet model created for $\mathbf{X}_{\text{A}i}$ is connected to layer L_i^t .

As an example, in the diagram below, we show the results of lines 7-9 of Algorithm 1 in a tree-form (we use $s = 2$). Each rectangle encapsulates the result of multiple possible decomposition, obtained from multiple bootstrap samples. For simplifying the explanation, we omit the distinction between ancestor and descendant sets. For example, in the top rectangle, \mathbf{X} is decomposed, using statistical independence tests of order n , in two ($s = 2$) manners: 1) $\{\mathbf{X}_1, \mathbf{X}_2, \mathbf{X}_3, \mathbf{X}_4\}$, 2) $\{\mathbf{X}_5, \mathbf{X}_6, \mathbf{X}_7\}$. Each set \mathbf{X}_i is further recursively decomposed using statistical independence tests of order $n + 1$. For example, \mathbf{X}_7 is decomposed in two manners (using different bootstrap samples).

B Complexity of BRAINet Structure Learning

The complexity of the proposed algorithm is essentially identical to that of the B-RAI algorithm. That is, $\mathcal{O}(n^k s^{k+1})$ conditional independence tests, and $\mathcal{O}(ns^k)$ Bayesian scoring function calls., where s is the number of splits, n is the number of input variables ($|\mathbf{X}|$), and k is the maximal order of conditional independence in the data.



The running-trace of RAI in the worst-case scenario is a single path in the GGT, and has a CI-test complexity of $\mathcal{O}(n^k)$, and the ratio between B-RAI and RAI is $\sum_{i=0}^k s^i$.

For the Bayesian scoring function, the complexity is $\mathcal{O}(ns^k)$, as only the leaves (when the exit condition is satisfied) are scored. Note that the worst-case scenario is the case where the true underlying graph is a complete graph, which is not typical in real-world cases. In practice, significantly fewer CI tests and scoring operations are performed.

C BRAINet Uncertainty Estimation

C.1 A Relation between Generative Uncertainty and Predictive Uncertainty

During the construction of a BRAINet model, multiple connectivity patterns at each point in the network are learned using different bootstrap samples. Thus, when the epistemic uncertainty of θ is high, connectivity patterns learned from different bootstrap samples are likely to be dissimilar. However, when the epistemic uncertainty of θ lowers (e.g., for a larger training set), the connectivity patterns for any two bootstrap samples are more likely to be similar, at which point the aleatoric uncertainty dominates, and further reducing epistemic uncertainty (e.g., by adding more training data) will not result in a reduction of the number of unique connectivity patterns.

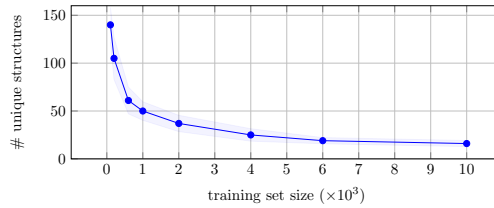


Figure 7: Number of unique structures (neural connectivity patterns) embedded in a single BRAINet ($s = 3$) for MNIST, as a function of the training set size. As the epistemic uncertainty increases (small training sets), more unique structures are automatically encoded in BRAINet, resulting in a broader prior over the network parameters. At the other end, as the training set size increases, the number of unique structures decreases and converges to a number greater than one, indicating the existence of an aleatoric uncertainty. Results are averaged over 5 experiments; error bars indicate standard deviation.

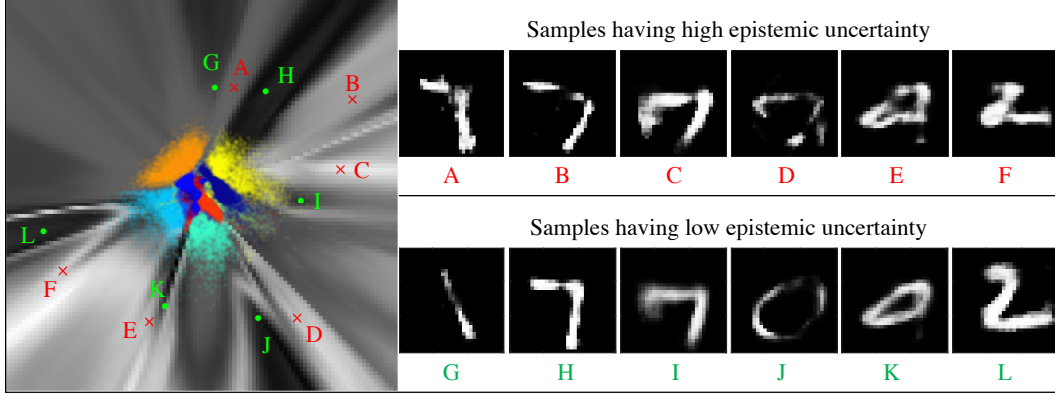


Figure 8: Epistemic uncertainty estimate using BRAINet ($s = 2$) as measured by mutual information, visualized on the latent space of a VAE on MNIST. In this experiment, as suggested by Smith & Gal [29], a VAE with latent space size 2 was trained and the axes are the values of these 2 latent variables. Brighter pixels correspond to a higher mutual information, i.e. a higher uncertainty. Images were then generated by setting values for each latent variable, 100 values in $[-10 : +10]$. Colored pixels correspond to the training data. As demonstrated, ambiguous images, $\{A, \dots, F\}$, yield high epistemic uncertainties, as opposed to the clearer images of $\{G, \dots, L\}$.

C.2 An example for Epistemic Uncertainty Estimation using MI Criterion

In this section we repeat the experiment described by Smith & Gal [29]. Result is in Figure 8, where we also plot 12 images generated by a VAE: 6 having low MI score, and 6 having high MI score.

D Experiments

This section contains tables and figures referenced in the paper. See captions for a detailed explanation.

Firstly, we wish to emphasize an important property of the BRAINet structure, which allows us to sample networks that are significantly smaller than the overall structure. This leads to a significantly smaller computational cost, during training and inference, than other methods. For example, in a BRAINet for MNIST, the average number of operations (multiply and add) during inference is $\sim 5.5\times$ smaller than other methods (and has $\sim 5.5\times$ fewer parameters to train each epoch). Moreover, in contrast to MC-dropout, which samples neurons from each layer, BRAINet samples full layers, making it computationally efficient using common hardware. In all our experiments, we report only the size of the *full* BRAINet structure and ignore the sizes of the sampled networks.

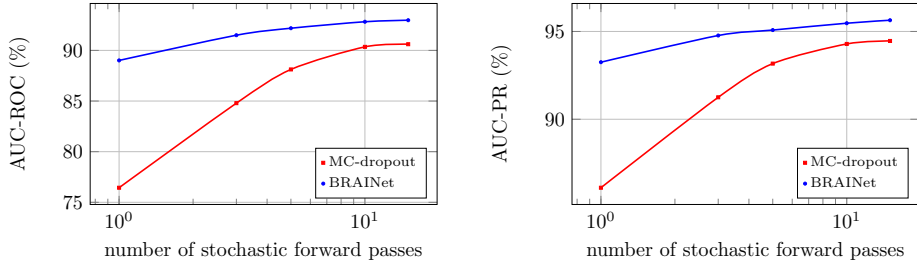


Figure 9: Area under ROC and precision-recall curves as a function of the number of stochastic forward passes. It is evident that BRAINet achieves high AUC even for a small number of forward passes, compared to MC-dropout. This result corresponds to the OOD-detection experiment described in Table 1 of the main paper. Architecture: ResNet20, in-distribution: CIFAR-10, OOD: SVHN.

Table 3: The effect of conditioning the discriminative function on a MAP estimation of a generative network (BRAINet) for Deep Ensembles [17]. Regression Benchmark datasets comparing RMSE and NLL.

DATASET	RMSE		NLL	
	ENSEMBLE	BRAINet+ENSEMBLE	ENSEMBLE	BRAINet+ENSEMBLE
CONCRETE	5.46 ± 0.52	4.17 ± 0.59	2.92 ± 0.16	2.56 ± 0.13
BOSTON HOUSING	2.90 ± 0.71	2.17 ± 0.56	2.37 ± 0.25	1.88 ± 0.21
POWER PLANT	4.11 ± 0.16	4.10 ± 0.14	2.82 ± 0.03	2.8 ± 0.03
YACHT	3.09 ± 1.03	1.10 ± 0.36	2.25 ± 0.39	1.09 ± 0.14
KIN8NM	0.09 ± 0.00	0.08 ± 0.00	-1.18 ± 0.02	-1.23 ± 0.03
ENERGY	0.95 ± 0.26	0.71 ± 0.10	1.16 ± 0.25	1.02 ± 0.13
NAVAL PROPULSION PLANT	0.00 ± 0.00	0.00 ± 0.00	-3.55 ± 0.06	-3.68 ± 0.05
WINE	0.64 ± 0.04	0.59 ± 0.05	0.92 ± 0.08	0.76 ± 0.05
PROTEIN	4.62 ± 0.17	4.16 ± 0.15	2.79 ± 0.03	2.60 ± 0.09

Table 4: The effect of conditioning the discriminative function on a MAP estimation of a generative network (BRAINet) for MC-dropout [6]. Regression Benchmark datasets comparing RMSE and NLL.

DATASET	RMSE		NLL	
	MC-DROPOUT	BRAINet+DROPOUT	MC-DROPOUT	BRAINet+DROPOUT
CONCRETE	4.83 ± 0.52	3.09 ± 0.78	2.92 ± 0.09	2.64 ± 0.12
BOSTON HOUSING	2.80 ± 0.52	1.90 ± 0.38	2.39 ± 0.15	2.16 ± 0.08
POWER PLANT	4.02 ± 0.18	4.00 ± 0.16	2.80 ± 0.05	2.79 ± 0.04
YACHT	1.42 ± 0.48	0.61 ± 0.25	1.60 ± 0.13	1.38 ± 0.06
KIN8NM	0.10 ± 0.00	0.08 ± 0.00	-0.95 ± 0.03	-1.10 ± 0.03
ENERGY	0.88 ± 0.13	0.56 ± 0.08	1.62 ± 0.03	1.44 ± 0.02
NAVAL PROPULSION PLANT	$(1.8 \pm 0.2)e^{-3}$	$(1.2 \pm 0.3)e^{-3}$	-4.22 ± 0.01	-4.35 ± 0.02
WINE	0.62 ± 0.04	0.54 ± 0.04	0.93 ± 0.06	0.82 ± 0.05
PROTEIN	3.60 ± 0.03	3.46 ± 0.19	2.69 ± 0.01	2.67 ± 0.03

Table 5: Comparison between BRAINet and various state-of-the-art methods on large networks. In all benchmarks, BRAINet achieves the lowest expected calibration error [9].

DATASET	MODEL	SGD	SWA	SWAG-DIAG	SWAG	KFAC-LAPLACE	SWA-DROPOUT	SWA-TEMP	BRAINet
CIFAR-10	VGG-16	0.0483	0.0408	0.0267	0.0158	0.0094	0.0284	0.0366	0.0090
CIFAR-10	PRERESNET-164	0.0255	0.0203	0.0082	0.0053	0.0092	0.0162	0.0172	0.0036
CIFAR-10	WRN28x10	0.0166	0.0087	0.0047	0.0088	0.0060	0.0094	0.0080	0.0040
CIFAR-100	VGG-16	0.1870	0.1514	0.0819	0.0395	0.0778	0.1108	0.0291	0.0247